DTIC® has determined on **10 / 7 /2010** that this Technical Document has the Distribution Statement checked below. The current distribution for this document can be found in the DTIC® Technical Report Database.

☑ **DISTRIBUTION STATEMENT A.** Approved for public release; distribution is unlimited.

☐ **© COPYRIGHTED**; U.S. Government or Federal Rights License. All other rights and uses except those permitted by copyright law are reserved by the copyright owner.

☐ **DISTRIBUTION STATEMENT B.** Distribution authorized to U.S. Government agencies only (fill in reason) (date of determination). Other requests for this document shall be referred to (insert controlling DoD office)

☐ **DISTRIBUTION STATEMENT C.** Distribution authorized to U.S. Government Agencies and their contractors (fill in reason) (date of determination). Other requests for this document shall be referred to (insert controlling DoD office)

☐ **DISTRIBUTION STATEMENT D.** Distribution authorized to the Department of Defense and U.S. DoD contractors only (fill in reason) (date of determination). Other requests shall be referred to (insert controlling DoD office).

☐ **DISTRIBUTION STATEMENT E.** Distribution authorized to DoD Components only (fill in reason) (date of determination). Other requests shall be referred to (insert controlling DoD office).

☐ **DISTRIBUTION STATEMENT F.** Further dissemination only as directed by (inserting controlling DoD office) (date of determination) or higher DoD authority.

Distribution Statement F is also used when a document does not contain a distribution statement and no distribution statement can be determined.

☐ **DISTRIBUTION STATEMENT X.** Distribution authorized to U.S. Government Agencies and private individuals or enterprises eligible to obtain export-controlled technical data in accordance with DoDD 5230.25; (date of determination). DoD Controlling Office is (insert controlling DoD office).

Damage Thresholds for Exposure to NIR and Blue Lasers in an In Vitro RPE Cell System

Michael L. Denton,[1] *Michael S. Foltz,*[1] *Larry E. Estlack,*[2] *David J. Stolarski,*[1] *Gary D. Noojin,*[1] *Robert J. Thomas,*[3] *Debbie Eikum,*[1] *and Benjamin A. Rockwell*[3]

PURPOSE. Until reliable nonanimal systems of analysis are available, animal models will be necessary for ocular laser hazard analysis and for evaluating clinical applications. The purpose of this work was to demonstrate the utility of an in vitro system for laser bioeffects by identifying photothermal and photochemical cytotoxicity thresholds for continuous-wave (cw) and mode-locked (ml) laser exposures.

METHODS. Exogenous melanosomes were added to hTERT-RPE1 cells in exposure wells 1 day before laser exposure. Thermal or photochemical laser exposures were delivered to artificially pigmented retinal pigment epithelial (RPE) cultures, with subsequent assay for viability 1 hour after exposure. Beam delivery for the 1-hour photochemical exposures was via a modified culture incubator. The cytoprotective effect of pretreatment with two antioxidants was investigated.

RESULTS. Phagocytosis of melanosomes by the RPE cells was efficient, yielding cultures of uniform pigmentation. The damage threshold for the thermal exposure was consistent with published in vivo results. Thresholds for both blue exposures (cw and ml) were identical. Overnight treatment of cells with ascorbic acid (AA) minimized cell death from both cw and ml blue laser exposure, whereas similar treatment with *N*-acetyl-L-cysteine (NAC) was less effective.

CONCLUSIONS. The in vitro system described is suitable for measuring meaningful thermal and photochemical laser damage thresholds. The system is also useful in comparative laser bioeffects studies, such as comparisons between cw and ml laser exposures, cells with various degrees of pigmentation, and studies determining the efficacy and mechanisms of treatments altering the response of cells to lasers. (*Invest Ophthalmol Vis Sci.* 2006;47:3065–3073) DOI:10.1167/iovs.05-1066

M any lasers in the military and in basic scientific research can achieve relatively high powers, raising concerns for human safety. This is particularly true of ocular hazards, where optics greatly magnify laser irradiances at the retina.[1-3] Due to the presence of intracellular melanosome granules, the retinal pigment epithelial (RPE) layer plays an important role in light absorption[4-6] and is thus a common site for pathologic involvement in ocular laser damage, especially from thermal mechanisms for laser wavelengths in the visible and near-infrared (NIR).

In many modern laser applications, mode-locked lasers are used because of multiphoton absorption produced from the high-peak powers in each pulse. The ANSI Z136.1 standard[7] on laser safety treats femtosecond mode-locked (ml) lasers with high-repetition frequency as being no more damaging to tissues than continuous-wave (cw) lasers of the same wavelength. This principle has been shown to hold true experimentally in conditions that lead to thermal damage from femtosecond[8] and picosecond[9,10] pulsed lasers. In the photochemical regime, however, there is the possibility of chemical effects by mode-locked beams at low average powers, given their higher photon densities. We have an interest in comparing the photo-oxidative responses of RPE cells to these lasers. Although there have been extensive studies on photochemical (actinic) damage caused by cw lasers and blue light,[4,11-14] there is no published report of mode-locked effects of chronic, low-level exposure to either the eye or skin.

The rationale for establishing safe exposure guidelines by safety committees is generally assessed by evaluation of damage thresholds and proposed mechanisms in nonhuman primate models. Methods for safety analysis without using animals are an important bridge between experiment and theory. Computer modeling and simulation of laser bioeffects, although gaining the acceptance of the safety community has only a validating role in the animal ED_{50} damage threshold data used by safety committees. Systems of in vitro analysis must be tested for a role in accurate damage evaluation and validation for computer simulations. In vitro systems allow accurate measures of optical transmittance of culture buffers and actual beam diameter delivered to cells, providing an advantage over animal studies.[15]

Laser bioeffects studies in RPE explant tissues have been reported,[6,16-18] where a relatively small piece of eye cup material (RPE layer on choroid) was used to generate a large number of measurements. With the use of RPE cell cultures, a single laser exposure per well of a microtiter plate is possible. This one-exposure-per-well method eliminates potential extracellular signaling between laser-exposed cells. Identifying cellular pathways involved in laser-tissue interactions using molecular technology, such as transcriptomics and proteomics, is more straightforward in a homogeneous cell type than in a complex tissue. Organ-derived RPE cells placed in culture originate from a complex tissue and lose their melanosomes by a dilution effect during expansion, which often results in cultures with sporadic pigmentation and contamination with non-RPE cells. We chose to work with an established RPE cell line because of its simplicity (cellular homogeneity and environmental manipulation) and consistency. The human-derived, hTERT-RPE1 cells used in our experiments were immortalized by transfection with the catalytic component of the human telomerase (*hTERT*) gene,[19] which does not induce changes associated with a transformed phenotype,[20] as is commonly
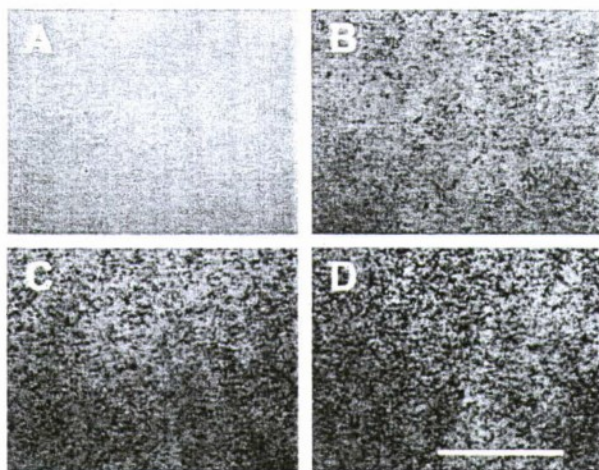
FIGURE 1. Artificial pigmentation of hTERT-RPE1 cells in culture. Bright-field micrographs of hTERT-RPE1 cells containing no added melanosomes (**A**), and approximately 77, 154, and 231 bovine melanosome particles per cell (**B-D**, respectively). All images were acquired and processed equally. Scale bar, 500 μm. Original magnification, $\times 100$.

found when using viral genes. In addition, these cells have been found to express many RPE-associated proteins.[21]

The purpose of this study was to use artificially pigmented RPE cells to determine in vitro irradiance thresholds (ED_{50}) for photothermal and photochemical laser damage, and to identify antioxidants capable of protecting these cells from laser-induced cell death.

MATERIALS AND METHODS

The human RPE cell line hTERT-RPE1 was purchased from BD-Clon-Tech (Palo Alto, CA) and is now available at the American Type Culture Collection (ATCC, Manassas, VA). Except for fetal bovine serum (Atlanta Biologicals, Atlanta, GA), the source for all cell culture media components and buffer solutions was MediaTech, Inc. (Herndon, VA). Calcein-AM (C-3099) and ethidium homodimer-1 (EthD1; E-1169) were purchased from Invitrogen (Eugene, OR). Bovine eyes were obtained from Animal Technologies (Tyler, TX).

Cell Culture and Pigmentation

Cultures of hTERT-RPE1 cells were maintained at standard conditions (37°C and atmosphere containing 5% CO_2) in complete medium (DMEM-F12 medium, 10 mM HEPES [pH 7.4], 10% fetal bovine serum, 1 mM glutamine, and antibiotics [100 IU $\cdot$ mL^{-1} penicillin, 100 μg $\cdot$ mL^{-1} streptomycin, and 50 μg $\cdot$ mL^{-1} gentamicin]). Cell stock cultures were grown in 75-cm^2 flasks, passaged at confluence (average split ratio of 1:10), and discontinued after 18 passages. Cells grown in 48-well microtiter plates were seeded in 0.3 mL growth medium at 70,000 (blue exposures) or 75,000 (NIR exposures) cells per well.

Melanosomes were isolated from bovine eye cups, as previously described.[22] Stock solutions of melanosome particles (MPs) were stored in 0.25 M sucrose (Sigma-Aldrich, St. Louis, MO) at -20°C. To quantify melanosome concentration in stock solutions, dilutions (1:50) in 0.25 M sucrose were counted (hemocytometer) by confocal microscopy (600$\times$ total magnification; FV300 configured on BX61WI; Olympus, Melville, NY). Concentrations of MP stocks used in the NIR and blue laser exposure studies were determined to be 2.94 ± 0.78 (SD) $\times 10^9$ MP $\cdot$ mL^{-1} and $2.72 \pm 0.34 \times 10^9$ MP $\cdot$ mL^{-1}, respectively. Melanosome densities of approximately 244 MP per cell (12-μL MP stock) and 160 MP per cell (8-μL MP stock) were used in the NIR and blue exposures, respectively. Images of artificially pigmented hTERT-RPE1 cells are shown in Figure 1.

On the second day after seeding, cells were rinsed twice with Hanks' balanced salt solution (HBSS) and prepared for counting, imaging, or laser exposure. Cell counts from six independent wells 2 days after seeding with 70,000 cells showed essentially one doubling whether there was no added MPs ($144,000 \pm 2,500$ cells per well) or 160 MPs were added per cell ($135,000 \pm 7,400$ cells per well).

During antioxidant experiments, cells received 2 mM ascorbic acid (AA; BP351-500; Fisher Scientific, Fair Lawn, NJ) or 1 mM *N*-acetyl-L-cysteine (NAC; A9165, Sigma-Aldrich) in fresh complete medium 18 to 20 hours before exposures. Ascorbic acid serves as a well-known physiological antioxidant in the RPE layer,[23,24] and efficiently scavenges free radicals.[25] Intracellularly, NAC is converted to glutathione (GSH), which can then provide antioxidant protection both directly (reducing oxidized forms of ascorbate, for example) and in enzyme-dependent pathways, for removing organic peroxides and electrophiles.[26]

Laser Exposures and Damage Assessment

Cells were always exposed 2 days after seeding in 48-well plates without lids. Immediately before laser exposure, cells in experimental and control wells were washed twice with 0.5 mL sterile HBSS and then exposed to the laser in 0.1 mL DMEM medium (without phenol red) supplemented with 2% bovine serum albumin (fraction V; Fisher Scientific), 1 mM glutamine, antibiotics (same as complete medium), and 10 mM HEPES buffer (pH 7.4; exposure medium). After exposure, the exposure medium was aspirated and replaced with 0.3 mL complete medium.

After 1 hour of recovery in the standard incubation conditions, control and laser exposed cells were rinsed with HBSS and stained (10 minutes at 37°C) for viability using 1.7 μM calcein-AM and 1.4 μM EthD1 in 0.1 mL HBSS, as previously described.[27] The exposure site was identified as either positively stained with EthD1 (band-pass exciter of 475–545 nm and a barrier filter at 590 nm) or as a region devoid of staining by calcein-AM (band-pass exciter of 460–490 nm and a band-pass emitter of 490–530 nm). Images (pseudocolor) of damage zones were viewed (blind of dosimetry) by three individuals and final scoring for yes/no damage required a consensus from two.

NIR Laser Exposures. Beam delivery to cells is depicted in Figure 2A. A titanium:sapphire laser (Mira 900F; Coherent, Palo Alto, CA) was used as our source for mode-locked exposures (Gaussian, 810 nm, 130 fs, 76 MHz). Beam diameter at the cells ranged from 104 to 110 μm, and in calculation of irradiance for an experiment we used the diameter measured during that experiment. To enhance laser damage detection we arranged seven individual exposures in a circular pattern (six surrounding one), each separated from each other by e^{-1} spacing distribution, generating an overall exposure diameter of approximately 266 μm. In this manner, we could attain very high irradiances used to assay cells without pigment in a separate study,[27] while achieving a pseudo flat-top profile with approximately 20% variance. We continued this practice in the present study.

Laser output power was adjusted using a half-wave plate (λ) and glan-laser prism (GP), and laser wavelength was confirmed by a spectrometer (Ocean Optics, Dunedin, FL). A daily power ratio was determined (power meter [Pm] 1 vs. Pm 2) such that power adjustment based on Pm 1 could be used to predict power at Pm 2 (and thus irradiance at the sample). Just before the cells, the laser was passed through a NIR-corrected long-working-distance microscope objective (Obj; 10$\times$, M Plan NIR, NA 0.26; Model 378823; Mitutoyo America Corp., Aurora, IL), facilitating knife-edge measurements of beam radius and real-time visual assessment of cells during laser exposure via a charge-coupled device (CCD) camera.

Blue-Laser Exposures. Beam delivery to cells is depicted in Figure 2B. Modifications (includes attachment to the laser table) were made to a standard cell culture incubator (model 320; Therma Forma, Marietta, OH), which allowed simultaneous delivery of the cw and mode-locked beams to the interior chamber. Microtiter culture plates were fixed to a breadboard suspended from the ceiling of the incuba-
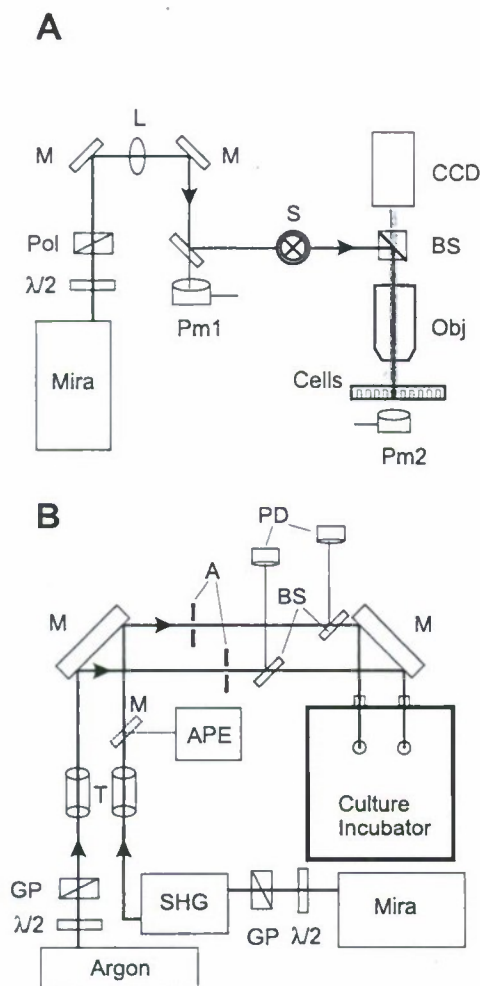
A

B

FIGURE 2. Experimental laser beam delivery for ml 810-nm (**A**) and 458-nm (**B**). The laser provided ml NIR (**A**) and ml blue (frequency-doubled, **B**) beams. A small-frame argon laser provided the blue cw beam. Cells (microtiter dishes) were exposed on the stage beneath the objective (Obj, **A**) or inside the incubator (**B**). $\lambda/2$, half-wave plate; GP, glan-laser prism; Pm, power meter; M, mirror; L, lens; S, shutter; AP, aperture; PD, photodiode; BS, beamsplitter; APE, autocorrelator; CCD, charge-coupled device camera.

tor. The laser provided the mode-locked beam and was tuned to 915.8 nm with the output directed into a frequency-doubling crystal (model 4500; Coherent) to obtain 115-fs pulses at 76 MHz with a wavelength of 457.9 nm at the sample. The pulse duration of the doubled output from the laser was determined with an autocorrelator (Pulse Check,

Berlin, Germany). The cw laser source (457.9 nm) was an argon ion laser (either model 168B-06; Spectra Physics, Mountain View, CA; or model 85; Lexel, Fremont, CA). Output profiles for both argon lasers were Gaussian.

A single-lens imaging system (400-mm focal length) was used to image each laser at an aperture (A), to produce a flat-top beam profile with a spot size of approximately 550 μm at the cells. Telescopes (T) were used to expand the beams to the back surface of the apertures, where only the central portion passed through to the sample. Focus and centering of the imaging system was checked using a beam profiler (Vision 1024; ThorLabs, Newton, NJ). To ensure the central location of the laser exposures within each well of the 48-well plates, metal discs having central 0.5-mm pinholes were inserted into the wells of an alignment plate. Adjustment of laser position was such that maximum power was transmitted through the pinholes to photodiodes placed directly beneath the wells (machined into the breadboard), guaranteeing reproducible beam location.

Laser output power was adjusted using a half-wave plate (λ) and glan-laser prism (GP), and laser wavelength was confirmed by a spectrometer (Ocean Optics). Power was measured before and after the experiment using a power meter (model 1830-C; Newport, Irvine, CA) and detector head (model 818-SL; Newport) located inside the incubator. Photodiodes (PD) tracked power variations during the course of the experiment and were used to determine average irradiance for exposures. Power measurements before and after each exposure were used to calibrate the real-time monitors.

Statistics

Uncertainty in our irradiance values was determined from calculated combined standard uncertainties (types A and B) for measuring both laser power and diameter at the sample.[28] We report expanded uncertainties in our irradiance values using a 95% confidence level (i.e., 2× SD). Damage threshold irradiance values (ED_{50}) were determined using the Probit[29] method. The Probit output includes additional uncertainty intervals (fiducial limits; FLs) related to the ED_{50} value, for which 95% confidence levels also were used. Table 1 summarizes our threshold results.

Computer Modeling

Supporting analyses of experimental results were provided using the Buffington-Thomas-Edwards (BTE) thermal model.[30,31] Absorption coefficients for cell monolayers without and with artificial pigmentation were calculated[32] from measured bulk absorbances (each of seven wells read in triplicate) using a microtiter plate reader (Genios model; Tecan USA., Research Triangle Park, NC). Absorbance filters were either 460 ± 5 or 810 ± 5 nm. An average absorbance for plate and medium alone was subtracted from average absorbances of plate, medium, and cells (with or without melanosomes). The subtractive analysis minimized the incorporation of surface reflection and absorption from media and well-plate into our measured absorption coefficients. A spectrometer (Ocean Optics) was used to measure absorption

TABLE 1. Phototoxicity (Threshold) Data for Laser Exposure to Artificially Pigmented RPE Cells

Exposure Condition	n	Probit Slope	ED_{50} $(J \cdot cm^{-2})$	Fiducial Limits (95% Confidence)	
				Lower	Upper
810 nm, 0.25 s, ml 130 fs, 76 MHz	45	11.5	1900 ± 307 (475 ± 77)	1610 ± 260	2150 ± 347
458 nm, 3600 s, cw	49	29.3	0.474 ± 0.070 (1,706 ± 252)	0.456 ± 0.067	0.496 ± 0.073
458 nm, 3600 s, ml 115 fs, 76 MHz	47	30.5	0.472 ± 0.066 (1,699 ± 236)	0.454 ± 0.063	0.493 ± 0.069

Data are expressed as irradiance ± extended uncertainty (W · cm^{-2}), which is defined as combined standard uncertainty × k, where $k = 2$ for 95% confidence.

TABLE 2. Thermal Properties of the Exposure Layers for Thermal Modeling

	Absorption Coefficient (1/cm)		Thermal Conductivity (W/cm/°C)	Density (g/cm³)	Specific Heat (J/g/°C)	Convective Heat-Transfer Rate (W/cm²/°C)	Emissivity	Refractive Index
	460 nm	810 nm						
Plastic Plate	0.464	0.602	2.00×10^{-3}	1.00	1.25	1.00×10^{-4}	1.00	1.57
Exposure Medium	0.581	0.385	4.28×10^{-3}	1.00	4.19	7.41×10^{-3}	0.98	1.33
hTERT-RPE1 Cells			6.28×10^{-3}	1.00	4.19	3.00×10^{-3}	0.80	1.33
Cells, No MP	12 ± 4* (10–15)†	6 ± 2* (5–10)†						
160 MP/Cell	480 ± 29* (395–610)†							
244 MP/Cell		519 ± 23* (427–661)†						

* Calculated using 7 μm thickness for cell layer.

† Range calculated for 8.5- or 5.5- μm thickness of cell layer, respectively.

of exposure medium (1-cm cuvette). Thickness of the bottom of well-plates (growth surface) was found to be 1.57 ± 0.02 mm (cross-sectional slicing). The absorption coefficient for the well-plate was computed using bulk absorbance readings from the microtiter plate reader. However, this value was probably an overestimate, as a subtractive method was not used.

The BTE thermal model numerically computed an approximate solution to the bioheat equation, expressed in cylindrical coordinates by equation 1. The solution to this initial value problem was performed using a finite-difference method for time-dependent partial differential equations.[33] The cell culture was modeled as a three-layer structure of essentially infinite radial extent. Layer axial dimensions representative of the measured values for cell culture media, cell monolayer, and well-plate used were 100 μm, 7 ± 1.5 μm, and 1.6 mm, respectively. Each layer was assumed to be homogeneous in optical and thermal properties, each of which is listed in Table 2. No losses by scattering were considered.

$$\rho c \frac{\delta v}{\delta t} = \frac{\kappa \delta v}{r \delta r} + \frac{\delta}{\delta r}\left(\kappa \frac{\delta v}{\delta r}\right) + \frac{\delta}{\delta z}\left(\kappa \frac{\delta v}{\delta z}\right) + A \qquad (1)$$

In equation 1, $v = v(z,r,t)$ represents the temperature rise (in Kelvin) in the cell culture and well-plate as a function of time and position, $A = A(z,r,t)$, is referred to as the source term and represents energy from the laser absorbed per unit time and volume (in J · cm^{-3} · s^{-1}), $\kappa = \kappa(z)$ is the thermal conductivity (in J · cm^{-1} · s^{-1} · K^{-1}), $c = c(z)$ is the specific heat of the layer (in J · g^{-1} · K^{-1}), $\rho = \rho(z)$ is the layer density (in g · cm^{-3}), with z specifying the axial coordinate in the tissue. For a cell culture sample, we assumed no perfusion and that the culture was in thermal equilibrium with the surrounding atmosphere.

For our model, the time-dependent solution to equation 1 was determined for a source term that provides a time-dependent description of the linear absorption of optical energy as a function of depth in the tissue, complete with spectral and radial dependence of energy being absorbed. Surface boundary conditions were addressed by an equation that is critical to the correct prediction of surface temperatures within the skin,[34] and includes a Lewis approximation.[35] The experiment modeled consisted of a layer of cell culture media covering a strongly absorbing monolayer of cells. This complete boundary condition ensured that the evaporative, radiative, and convective energy losses were correctly incorporated into the analysis.

Damage to the tissue was evaluated through the Arrhenius damage integral[34] given by equation 2:

$$\Omega(z,r) = C \int_{t_1}^{t_2} \exp\left(\frac{-E}{RT}\right) dt \qquad (2)$$

In equation 2, R is the universal gas constant, T represents the absolute temperature of a given coordinate at a given time, $T(z,r,t)$, and t_1 and t_2 represent the initial and final simulation times used in the solution of equation 1. The variable C is a normalizing rate constant (in seconds) and E the activation energy for a reactive process (in J · mole^{-1}). Values for C and E are reported in the literature[34] and are based on differing assumptions about tissue type and geometry. Without empirically determined values for C and E specific to our cell culture system, we chose to use 1×10^{44} · s^{-1} and 2.93×10^{5} J · mole^{-1}, respectively.[5,34] Values of this damage integral approaching $\Omega = 1$, indicate irreversible thermal damage to the cells at a given location for our study. Overall, our choice in selected constants and threshold parameters were consistent with established models in the literature that have been experimentally validated.[36,37]

RESULTS

Artificial Pigmentation of hTERT-RPE1 Cells

Given that the hTERT-RPE1 cells retained their phagocytic phenotype in culture, we were able to generate artificially pigmented RPE cells suitable for laser bioeffects experiments by simple addition of MP to culture medium. Uptake of the melanosomes by the human hTERT-RPE1 cells was rapid, typically within 4 hours. Madin-Darby canine kidney (MDCK) epithelial cells were very inefficient at uptake of exogenously added melanosomes (not shown), exemplifying how the hTERT-RPE1 cells have retained their differentiation-specific program for phagocytosis. Figure 1 shows bright-field micrographs of cells 1 day after pigmentation with previously isolated bovine melanosomes. Figure 1A depicts cells without added melanosomes, demonstrating a lack of light-contrasting material. Figures 1B–D illustrate that a greater degree of overall pigmentation was achieved by adding more exogenous melanosomes and that this pigmentation was spread more or less uniformly among the cells of the culture. The melanosomes localized to the cytoplasm of the hTERT-RPE1 cells, as individual nuclei of cells were evident as circles of excluded pigmentation. Rigorous adherence to the given cell culture schedule provided cell cultures with consistent pigmentation and outstanding overall viability. Viability of cells (pigmented or not) in the 48-well plate 2 days after seeding, determined by EthD1 and calcein-AM staining ($n = 5$), was found to be greater than 99% at the interior of the wells (4× field of view). Cells at the extreme periphery of the wells were less adherent than those in the center. This effect was minimized when using Falcon brand plates (model 353078; BD Biosciences, Franklin Lakes, NJ).

FIGURE 3. Damage assessments (fluorescent indicator dyes) for exposure to acute NIR and chronic blue lasers. Artificially pigmented cells exposed to 0.25-second, 810-nm ml laser at 1791 $W \cdot cm^{-2}$ (A) and 2950 $W \cdot cm^{-2}$ (B). Artificially pigmented cells exposed to 3600-second, 458-nm ml laser at 0.472 $W \cdot cm^{-2}$ (C) and 0.581 $W \cdot cm^{-2}$ (D) or cw laser at 0.484 $W \cdot cm^{-2}$ (E) and 0.596 $W \cdot cm^{-2}$ (F). Cells without added melanosomes exposed to 3600-second 458-nm cw laser at 0.811 $W \cdot cm^{-2}$ (G) and ml laser at 0.899 $W \cdot cm^{-2}$ (H). Scale bars: (A, B) 250 μm; (C–H) 500 μm.
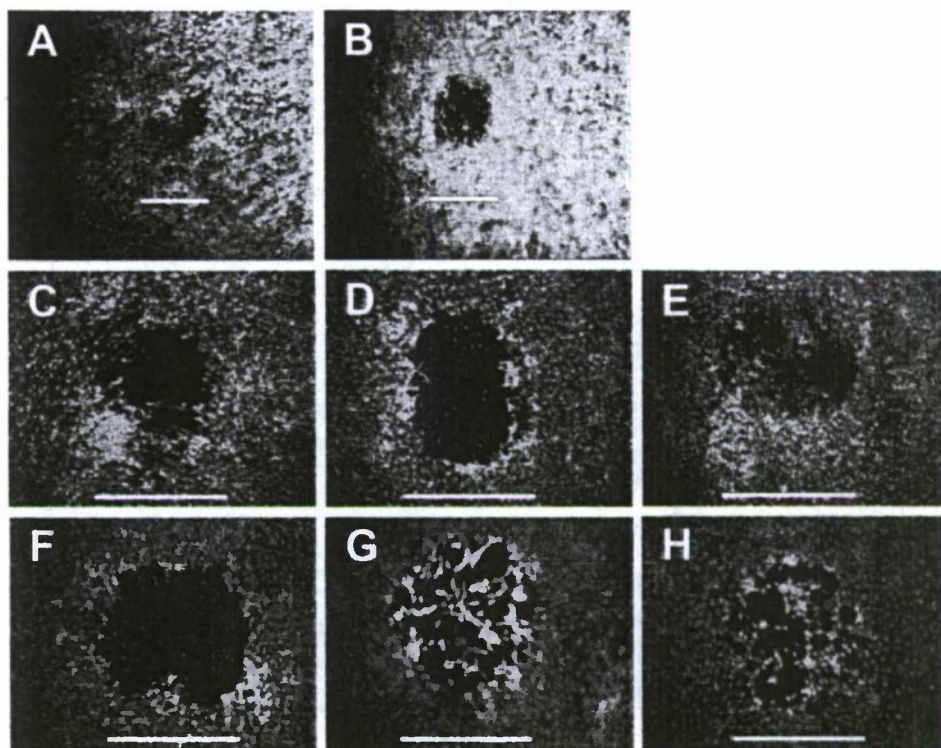
Acute NIR Laser Damage

Viability data from 45 exposures (0.25 seconds and 810 nm) were analyzed statistically using Probit software, the results of which are summarized in Table 1. Both the irradiance extended uncertainty and the probit fiducial limits (FLs) were calculated using 95% confidence intervals. The ED_{50} was calculated to be $1900 \pm 307 \, W \cdot cm^{-2}$, from which the lower and upper FLs varied by 15% and 13%, respectively. The value (11.5) for the Probit slope (Δprobability $\div$ Δdose at a probability of 0.5) was typical of slopes generated by data taken in minimal visible lesion (MVL) studies performed in vivo (Ref. 8, for example).

Cell damage from exposure to an ml 810-nm laser at irradiances equivalent to threshold (Fig. 3A) and 155% of threshold (Fig. 3B) showed a typical red damage zone (dead cells) with a surrounding green background (live cells). Damage zones from the higher irradiances were circular, due to damage from all seven individual exposures making up the overall exposure region. At lower irradiances, damage zones took on the appearance of various shapes corresponding to variable cytotoxicity within the seven individual exposures making up the overall exposure region.[27]

Chronic Blue Laser Damage

Artificially Pigmented Cells. Table 1 summarizes the experimental parameters for the blue laser exposures, along with the statistical (Probit) analyses of the viability data generated from fluorescence staining. The calculated ED_{50} irradiances for the ml (average irradiance) and cw exposures were statistically identical (0.472 and 0.474 $W \cdot cm^{-2}$), having very narrow ranges of FLs (4% from respective ED_{50} values) and Probit slopes of 30 (Δprobability $\div$ Δdose). Uncertainties in measuring irradiance are calculated to be ~15%, based on the measurements of beam spot size and average irradiance over the course of the 60-minute exposures.

Damage zones from exposure at threshold irradiances were less distinct (intermixed live and dead cells within the single,

large exposure site) for these blue, chronic exposures (Figs. 3C, 3E) compared with those from acute NIR exposure. At higher irradiances (e.g., 123% of threshold), the damage zones were more clearly demarcated (Figs. 3D, 3F) and were approximately the size of the laser beams.

Cells without Pigment. Our results with the melanosome-free cells were sporadic and precluded the calculation of an ED_{50} using Probit. For example, within our data set for cells without pigment ($n = 18$ cw and $n = 19$ ml), the highest irradiance leading to no damage was 54% greater than the lowest irradiance leading to positive damage. For the artificially pigmented cells, this crossover spread was only 14%. Figures 3G and 3H provide images of cells lacking pigment exposed to ml and cw blue beams at relatively high irradiances (191% and 171% of ml and cw thresholds in pigmented cells, respectively), showing a different appearance of damage compared with pigmented cells. The spattered appearance of green fluorescence was due to the lack of adherent cells. In addition, the calcein-AM staining was enhanced (increased fluorescence) in nonpigmented cells affected by the blue laser. These observations would collectively indicate a role for the melanosomes in the cellular damage from the blue lasers, but the nature (thermal and photochemical or purely photochemical) and the extent of this role could not be addressed by our viability end points.

Cytoprotection from Photochemical Damage by AA and NAC. To provide further evidence for substantial oxidation during exposure to both the ml and cw laser at 458 nm, we show protection from cell death by pretreatment of the cells with the antioxidant, AA. We assessed (as for laser damage) cell toxicity of overnight incubation in AA by manually counting dead cells per field of view in the center of the wells, and found no loss of viability due to toxic effects of 2 mM AA. The range of laser irradiances for the AA-treated series was 0.482 to 0.604 $W \cdot cm^{-2}$ and 0.495 to 0.612 $W \cdot cm^{-2}$ for cw and ml exposures, respectively. To ensure proper control, we exposed cells that had only media exchange at the time exper-

TABLE 3. Protection of RPE Cells from Laser-Induced Photochemical Death by Overnight Pretreatment with Ascorbic Acid (AA) and N-acetyl-l-cysteine (NAC)

	CW Laser				Mode-Locked Laser		
Media Control	2 mM AA	1 mM NAC	ED_{50} Data Range	Media Control	2 mM AA	1 mM NAC	ED_{50} Data Range
0.475 Y	0.482 N	0.468 N	0.481 Y	0.495 Y	0.495 N	0.481 N	0.493 Y
0.477 Y	0.483 N	0.485 N	0.482 Y	0.495 Y	0.497 N	0.490 Y	0.502 Y
0.498 Y	0.484 N	0.487 N	0.484 Y	0.495 Y	0.502 N	0.494 N	0.502 Y
0.503 Y	0.497 N	0.489 N	0.484 Y	0.497 Y	0.503 N	0.495 Y	0.511 Y
0.504 Y	0.497 N	0.495 N	0.496 N	0.498 Y	0.507 N	0.497 N	0.513 N
0.508 Y	0.503 N	0.501 N	0.497 N	0.504 Y	0.511 N	0.501 Y	0.515 N
0.517 Y	0.517 N	0.502 N	0.502 Y	0.510 Y	0.511 N	0.511 Y	0.517 Y
	0.525 N	0.507 N	0.504 Y		0.524 N		0.525 Y
	0.538 N		0.505 Y		0.531 Y		0.529 Y
	0.578 N		0.510 Y		0.532 N		0.529 Y
	0.583 Y		0.521 Y		0.612 Y		0.531 Y
	0.604 Y		0.522 N				
			0.532 Y				
			0.534 Y				
			0.537 Y				
			0.538 Y				

Irradiance of exposure (W · cm^{-2}). Y and N denote presence of damage.

imental wells received AA in fresh medium. As shown in Table 3, overnight pretreatment with 2 mM AA protected the artificially pigmented hTERT-RPE1 cells from blue cw (damage ratio of 0/7 vs. 7/7 in the controls) and ml (0/7 vs. 7/7 in the controls) laser-induced death for the irradiance range established by the controls (0.475–0.517 W · cm^{-2}).

Also given in Table 3 is comparable cytotoxicity data for a subset of irradiances used in our ED_{50} determination (ED_{60}–ED_{95} [0.481–0.538 W · cm^{-2}] and ED_{75}–ED_{94} [0.493–0.538 W · cm^{-2}] estimated for cw and ml, respectively). For each irradiance subset, all ED_{50} data are listed in the table. Over these irradiances, AA provided substantial protection from phototoxicity by cw (0/9 vs. 13/16) and ml (1/10 vs. 9/11) exposure. In one instance, 2 mM AA blocked the cytotoxicity of a cw irradiance of 0.578 W · cm^{-2} (note that the ED_{99} is estimated to be 0.563 W · cm^{-2}).

We explored the role of cellular glutathione in the response to blue lasers by assessing any protective advantage from overnight pretreatment with 1 mM of the precursor molecule, NAC. We found no loss of viability due to toxic effects of 1 mM NAC; however, overt cytotoxicity was observed when cells were incubated overnight in 5 mM NAC. The same media control data and ED_{50} data subsets used to assess the cytoprotective effects AA were used in the evaluation of 1 mM NAC (Table 3). The range of laser irradiances for the NAC-treated series was 0.468 to 0.507 W · cm^{-2} and 0.481 to 0.511 W · cm^{-2} for cw and ml exposures, respectively. For cw exposures, cytoprotection by NAC was fairly obvious (0/7 positives versus 6/6 [media control] and 8/10 [ED_{50} subset range]). However, when exposed to the ml laser, no clear distinction between NAC-treated and control cells could be made.

Computer Modeling of Laser Damage

Physical and laser parameters described in the experimental configuration and Table 2 were used to determine computer simulated threshold ED_{50} irradiances, with their associated maximum temperature increase and damage-zone size, for each of four exposure conditions (Table 4). Here we used a convergence criterion of ±5% and a predetermined damage-zone radius of 137.5 and 37.8 μm for the 458- flat-top and 810-nm Gaussian beams, respectively. As expected, predicted thresholds for nonpigmented cells where higher than for pigmented cells (5-fold for chronic and 33-fold for acute). The maximum temperature rise and damage radius values showed no dependence on pigment, indicating the program runs were consistent. In comparison with the measured thresholds (Table 1 and top line in Table 4), the model fell short in both the chronic- and acute-exposure conditions. The disparity in the chronic 458-nm exposure condition (29-fold overestimate) can be justified considering the fact that photochemical damage is expected to predominate. The fivefold underestimation by the model for the acute 810-nm exposure condition requires additional evaluation, as this disparity cannot be accounted for

TABLE 4. Results of Thermal Modeling and Computer Simulations

	3600 s Exposure 458 nm		0.25 s Exposure 810 nm	
	160 MP/Cell	No MP	244 MP/Cell	No MP
Measured ED_{50} (W · cm^{-2}) from Table 1	0.473	NA	1,900	NA
Predictions from BTE thermal model				
Computed ED_{50} (W · cm^{-2})	13.6	69.2	487	14432
Temp rise at computed ED_{50} (°C)	13.0	15.1	122.5	112.3
Maximum damage zone size (μm)	137.9	132.6	49.23	50.04
Temp. rise at measured ED_{50} (°C)	0.313	N/A	478.2	N/A
Damage zone radius at measured ED_{50} (μm)	0	N/A	135.6	N/A

solely by uncertainties in our measured irradiance. Considerations and potential modifications to the computer model are described in the Photothermal Discussion section.

Table 4 also lists the calculated maximum temperature increase and damage-zone size, with each of the two measured irradiance ED_{50} thresholds as input parameters. Evident are the same trends as seen for the computed thresholds. The maximum temperature increase in the chronic exposures to blue lasers is predicted to be only 0.3°C, whereas no thermal damage was predicted (no damage-zone radius estimate). This again leads to the unambiguous conclusion that cellular damage under these experimental conditions was photochemical in nature. Although the computed damage-zone radius for the acute NIR exposure was not out of the ordinary, the predicted 480°C maximum temperature increase from a 0.25-second exposure to 1900 W · cm^{-2} irradiance was unexpectedly high.[4] This too is discussed in a later section.

DISCUSSION

Importance of In Vitro Laser Damage Assessment

Without years of rigorous testing, data taken from laser damage studies performed in vitro cannot simply replace those obtained in animal models. Initially, a well-defined cell culture system could be used in validating the utility of computer-based predictions of laser bioeffects, to include estimations of damage thresholds. The ease with which cell environment and laser exposure parameters can be varied in an in vitro system facilitates the rapid validation of model predictions. Complex aspects of laser-tissue interactions, such as time-temperature history profiles and cell recovery from sublethal damage, can be evaluated quickly. The cell culture model alone would have its greatest utility in the study of basic cellular mechanisms for laser-tissue interactions (e.g., biochemical pathways involved), as well as in comparative studies, such as specific bioeffects of ml and cw beams.

The use of either RPE–choroid explants or primary RPE cells in culture would be ideal as an in vitro system, except that the availability of human and nonhuman primate (NHP) tissues is limited for many researchers. Contamination of cultures with non-RPE cell types can also occur. Artificial pigmentation of cultured RPE cells allows flexibility in the degree of pigmentation. The concept that RPE cells can internalize melanosomes is not novel. For example, Boulton and Marshall[38] developed a repigmentation method for human RPE cells where human eyes were the source for both RPE cells (which lose their pigment by repeated cell divisions) and melanosomes. Using electron microscopy, these authors observed that the pigment granules within the repigmented cells were randomly localized in the cytoplasm, did not aggregate, and were resistant to cellular lysis over a 7-day postchallenge period. Nonavailability of human eye tissues precludes this method for use in routine laser bioeffect studies.

Human RPE cells stably transfected with the catalytic component of hTERT have been generated,[19] establishing a human RPE cell line by a mechanism of telomere extension rather than by use of viral genes. As is the case for all RPE cells grown in culture, these immortalized cells have lost their pigmentation on repeated subculture. Our use of bovine melanosomes in conjunction with the human hTERT-RPE1 cell line does not increase demand for animal or human tissues, because bovine eyes were obtained from a beef-packing plant and the RPE cells were established in 1998. For laboratories with sources to human or NHP eyes, substituting melanosomes from these sources would provide additional validation to in vitro studies.

Consistent RPE monolayers with good overall viability were obtained by strict adherence to a fixed culture schedule. This

system will facilitate the study of human RPE bioeffects at the metabolic, genomic, and proteomic level while eliminating the need for primary human tissues, except in future validation experiments. Although we do not know the chemical effects of having bovine melanosomes within the human cells, we expect there to be little or no effect on these types of analyses. Cell culture parameters may be changed to approximate dosimetry values from animal studies.

Because the melanosomes were encased in cellular membrane (phagosomes), their chemistry may be different or obstructed compared with melanosomes endogenously assembled. This presents a potential drawback to our system. However, the absorption and heat dissipation properties of the melanosomes are probably unaffected by any membranous layers, and the use of our system in photothermal damage should be straightforward.

With its well-recognized role in age-related macular degeneration, lipofuscin-dependent oxidative damage of the RPE from broadband blue light has been documented.[39–42] In future investigations, in vitro samples with various concentrations of exogenously added melanosomes, lipofuscin granules, or melanolipofuscin granules could be generated for analysis, creating cells more closely resembling native RPE cells from humans at various ages.

In Vitro Photothermal Damage Threshold (810 nm)

Considering our choice in laser parameters and the pigmented state of the cultured cells, these acute exposures are expected to be thermal in nature.[7] In a prior investigation, we found no difference in thresholds between 800-nm ml and cw 0.25-second exposures in vivo.[8] This suggests that exposure of pigmented cells in vitro to the ml 810-nm beam causes damage by a thermal mechanism. Comparison of our in vitro threshold (1900 W · cm^{-2}) to that (0.024 W total intraocular energy) of the MVL study[8] is complicated by an inability to measure spot size directly in vivo. However, we calculate that a retinal spot size of 40 μm results in an MVL threshold irradiance equivalent to our in vitro irradiance threshold (assuming ocular transmittance of 0.9). This retinal spot size is a reasonable estimate for a collimated, 800-nm laser beam, which would suffer some chromatic aberrations in the eye.[15] This rationale validates the use of this artificially pigmented hTERT-RPE1 system for photothermal damage mechanisms, and supports the notion that the membrane encasement of the melanosomes (phagosomes) did not greatly affect their absorption properties, as proposed earlier.

The predicted threshold (487 W · cm^{-2}) and extreme temperature increase (478°C) predicted by the BTE thermal model (Table 4) indicate the need to evaluate the relevance of our input parameters in relation to the cell culture model. Admittedly, our measurements of bulk absorbance for calculating absorption coefficients were not precise, and did not rigorously account for scattering. An overestimate of absorption coefficient would result in an increase in predicted thermal absorption and subsequent temperature increase for a given irradiance, albeit not by an order of magnitude. It is possible that the model inadequately accounts for the sparse distribution of the intracellular melanosomes in our cell cultures, in opposition to the dense layer of melanosomes in the retina. There could be substantial error in the values listed (Table 2) for thermal properties of the plastic culture dish, as they are figures reported in the literature and on the Internet that do not necessarily describe the physical state found in the labware. Accurate measurements are in progress for future modeling in our laboratory.

In addition, the values used for the rate process terms (C and E) of equation 2 can have a major impact on the predicted

outcomes of the thermal model. Where we have relied on values in the literature that are derived from in vivo analyses, they may not accurately describe the processes occurring in our in vitro system. We are presently defining these values for our artificially pigmented hTERT-RPE1 cells for continuing laser bioeffects work.

Finally, we considered the effects of multiple exposures to a single location due to our laser exposure pattern of seven individual sites. The individual sites were spaced as described in the Methods section. We attempted to bound the effect of multiple exposures in our model by simulating a 0.5-second exposure, representing a worst-case scenario for a given exposure site, which lowered the predicted damage threshold by approximately 15%. We consider this a lower boundary to our estimated thresholds.

In Vitro Photochemical Thresholds (458 nm)

Using our artificially pigmented system, we found the damage thresholds for exposure to chronic ml and cw blue lasers to be identical. The threshold of $0.472 \text{ W} \cdot \text{cm}^{-2}$ average irradiance corresponds to a peak irradiance of $51,750 \text{ W} \cdot \text{cm}^{-2}$ (115 fs, 76 MHz), which was insufficient, over the course of a 1-hour exposure, to enhance cytotoxicity relative to cw exposure. Probit analyses (steep ED_{50} Δprobability $\div$ Δdose slopes) indicate that the cytotoxic response of our artificially pigmented RPE cells to blue laser exposure was more deterministic (all or nothing) than probabilistic. We interpret the qualitative difference in cytotoxicity staining between nonpigmented and pigmented cells (Fig. 3) to indicate a role for melanosomes in blue laser–induced damage in vitro, which confirms the view that melanin plays an important role in photochemical damage mechanisms in the native retina.[11,12] Although the beam diameters in our study were roughly the same as those used in a previous study in rhesus monkeys,[12] it is difficult to compare our results to those of Ham et al.[12] for several reasons. Our beam profiles were flat topped and our damage assessment was at 1 hour after exposure. The animal study used TEM_{oo} beams with 48-hour postexposure assessment. We are presently pursuing different end points of analysis (indicating apoptosis) for damage assessment in our in vitro model at postexposure recovery times greater than 1 hour.

The results from the thermal model (Table 4) support the conclusion that our in vitro cell cultures can provide a venue for studying photochemical damage mechanisms. Even if our thermal model underestimated the maximum temperature increase at our measured threshold irradiance (0.3°C) by a factor of 10, an increase of 3°C is still within the guidelines used for photochemical damage mechanisms.[4]

Reducing Photochemical Lethality with Antioxidants

Our results indicate a reduction in death, at normally lethal irradiances, when cells were preconditioned with modest concentrations of either AA or NAC. Overnight pretreatment with 2 mM AA efficiently protected cells from both cw and ml exposure, whereas pretreatment with 1 mM NAC appeared to be more efficient at protecting cells against cw than ml exposure. Although the full degree of protection (ED_{50}) from these antioxidants is yet to be determined, our results suggest a different mechanism of cytotoxicity (oxidation) for chronic blue cw and ml laser exposure.

One possible mechanism for this laser mode-specific effect could involve the production of different reactive oxygen species (ROS) during ml and cw exposures. AA has been shown to scavenge free radicals efficiently.[25] On conversion to glutathione (GSH) in cells, NAC provides antioxidant protection against hydroperoxides.[43] Further support for a dual role for

AA and NAC in the defense against oxidation comes from a study showing that AA provides substantial protection against death from hydrogen peroxide treatments in cells depleted of GSH.[44] It is conceivable that ml and cw exposure (chronic blue) generates the same free radical(s), but different sets of hydroperoxides. Perturbations in the activity of glutathione-*S*-transferases (GSTs), important enzymes in the metabolism of GSH, would also have effects on a cell's ability to quench hydrogen peroxides.[45] Further studies are required to elucidate any differences in ROS produced by the two types of lasers.

References

1. Ham WT Jr, Clarke AM, Geeraets WJ, Cleary SF, Mueller HA, Williams RC. The eye problem in laser safety. *Arch Environ Health.* 1970;20:156–160.

2. Beatrice ES, Randolph DE, Zwick H, Stuck BE, Lund DJ. Laser hazards: biomedical threshold investigations. *Mil Med.* 1977;14: 889–892.

3. Sliney DH, Wolbarsht ML. *Safety with Lasers and Other Optical Sources.* New York: Plenum Publishing; 1980.

4. Ham WT Jr, Ruffolo JJ Jr, Mueller H, Guerry D III. The nature of retinal radiation damage: dependence on wavelength, power level and exposure time. *Vision Res.* 1980;20:1105–1111.

5. Birngurber R, Hillenkamp F, Gabel V-P. Theoretical investigation of laser thermal retinal injury. *Health Phys.* 1985;48:781–796.

6. Brinkmann R, Huttmann G, Rogener J, Roider J, Birngruber R, Lin CP. Origin of retinal pigment epithelium cell damage by pulsed laser irradiance in the nanosecond to microsecond time regimen. *Lasers Surg Med.* 2000;27:451–464.

7. ANSI. *Safe Use of Lasers.* Orlando, FL: American National Standards Institute; 2000:Z-136.1–2000.

8. Thomas RJ, Noojin GD, Stolarski DJ, et al. A comparative study of retinal effects from continuous wave and femtosecond mode-locked lasers. *Lasers Surg Med.* 2002;31:9–17.

9. Courant D, Fritsch P, Naudy-Vives C, et al. Histological study of retinal damages induced by multiple picosecond pulses. *J Laser Appl.* 1998;10:229–231.

10. Courant D, Naudy-Vives C, Perot J-C, Garcia F, Dormont D. Experimental determination of retinal damage thresholds induced by multiple picosecond laser pulses. *J Laser Appl.* 1999;11:190–193.

11. Ham WT Jr, Ruffolo JJ Jr, Mueller HA, Clarke AM, Moon ME. Histologic analysis of photochemical lesions produced in rhesus retina by short-wavelength light. *Invest Ophthalmol Vis Sci.* 1978; 17:1029–1035.

12. Ham WT Jr, Mueller HA, Ruffolo MJ Jr, Clarke AM. Sensitivity of the retina to radiation damage as a function of wavelength. *Photochem Photobiol.* 1979;29:735–743.

13. Ham WT Jr, Mueller HA. The photopathology and nature of the blue light and near-UV retinal lesions produced by lasers and other optical sources. In: Wolbarsht ML, ed. *Laser Applications in Medicine and Biology.* New York: Plenum Publishing; 1989:191–246.

14. Stuck BE. The retina and action spectrum for photoretinitis ("blue-light hazard"). In: Matthes R, Sliney D, eds. *Measurements of Optical Radiation Hazards.* Vienna, VA: CIE; 1998:193–208.

15. Rockwell BA, Hammer D, Kennedy P, et al. Retinal spot size with wavelength. *Proc SPIE.* 1997;2975:148–154.

16. Kelly MW. *Intracellular Cavitation as a Mechanism of Short-Pulse Laser Injury to the Retinal Pigment Epithelium.* Medford, MA: Tufts University; 1997. Thesis.

17. Roegener J, Brinkmann R, Lin CP. Pump-probe detection of laser-induced microbubble formation in retinal pigment epithelium cells. *J Biomed Opt.* 2004;9:367–371.

18. Schuele G, Rumohr M, Huettmenn G, Brinkmann R. RPE damage thresholds and mechanisms for laser exposure in the microsecond-to-millisecond time regimen. *Invest Ophthalmol Vis Sci.* 2005;46: 714–719.

19. Bodnar AG, Ouellette M, Frolkis M, et al. Extension of lifespan by introduction of telomerase into normal human cells. *Science.* 1998;279:349–352.

20. Xu-Rong J, Jimenez G, Chang E, et al. Telomerase expression in human somatic cells does not induce changes associated with a transformed phenotype. *Nat Genet.* 1999;21:111-114.

21. Rambhatla L, Chiu C-P, Glickman RD, Rowe-Rendleman C. In vitro differentiation capacity of telomerase immortalized human RPE cells. *Invest Ophthalmol Vis Sci.* 2002;43:1622-1630.

22. Dontsov AE, Glickman RD, Ostrovsky M. Retinal pigment epithelium pigment granules stimulate the photo-oxidation of unsaturated fatty acids. *Free Radical Biol Med.* 1999;26:1436-1446.

23. Woodford BJ, Tso MOM, Lam K-W. Reduced and oxidized ascorbates in guinea pig retina under normal and light-exposed conditions. *Invest Ophthalmol Vis Sci.* 1983;24:862-867.

24. Lai Y-L, Fong D, Lam K-W, Wang H-M, Tsin ATC. Distribution of ascorbate in the retina, subretinal fluid and pigment epithelium. *Curr Eye Res.* 1986;5:933-938.

25. Bielski GHJ, Richter HW. Some properties of the ascorbate free radical. *Ann NY Acad Sci.* 1975;258:231-237.

26. Jones DP, Brown LA, Sternberg P. Variability in glutathione-dependent detoxification *in vivo* and its relevance to detoxification of chemical mixtures. *Toxicology.* 1995;105:267-274.

27. Denton ML, Eikum DM, Noojin GD, et al. Pigmentation in NIR laser tissue damage. *Proc SPIE.* 2003;4953:78-84.

28. Taylor BN, Kuyatt CE. Guidelines for evaluating and expressing the uncertainty of NIST measurement results. *NIST Tech Note.* 1297: 1994.

29. Finney DJ. *Probit Analysis.* New York: Cambridge University Press; 1971.

30. Thomas RJ, Buffington GD, Irvin LJ, et al. Experimental and theoretical studies of broadband optical thermal damage to the retina. *Proc SPIE.* 2005;5688:411-422.

31. Thomas RJ, Cain CP, Noojin GD, et al. Extension of thermal damage models of the retina to multi-wavelength sources. *Proc ILSC.* 2005;77-83.

32. Smith WJ. Optical materials and interference coatings. In: Fisher RJ, Smith WJ, eds. *Modern Optical Engineering.* New York: McGraw Hill Inc.; 1990:161-163.

33. Mainster MA, White TJ, Tips JH, Wilson PW. Transient thermal behavior in biological systems. *Bull Math Biophys.* 1970;32:303-314.

34. Welch AJ, Van Gemert M. *Thermal Response of Tissue to Optical Radiation.* New York: Plenum Press; 1995.

35. Torres JH, Motamedi M, Pearce JA, Welch AJ. Experimental evaluation of mathematical models for predicting the thermal response of tissue to laser irradiation. *Appl Opt.* 1993;32:597-606.

36. Welch AJ, Priebe LA, Forster LD, Gilbert R, Lee C, Drake P. Experimental validation of thermal retinal models of damage from laser radiation. University of Texas; Contract 1978;F33615-76-C-0605.

37. Welch AJ, Polhamus GD. Measurement and prediction of thermal injury in the retina of the rhesus monkey. *IEEE Trans Biomed Eng.* 1984;BME-31:633.

38. Boulton M, Marshall J. Repigmentation of human retinal pigment epithelial cells *in vitro. Exp Eye Res.* 1985;41:209-218.

39. Rozanowska M, Jarvis-Evans J, Korytowski W, Boulton ME, Burke JM, Sarna T. Blue light-induced reactivity of retinal age pigment. *J Biol Chem.* 1995;270:18825-18830.

40. Winkler BS, Boulton ME, Gootsch JD, Sternberg P. Oxidative damage and age-related macular degeneration. *Mol Vis.* 1999;5:32-42.

41. Cai J, Nelson KC, Wu M, Sternberg P Jr, Jones DP. Oxidative damage and protection of the RPE. *Prog Retin Eye Res.* 2000;19: 205-221.

42. Sparrow JR, Boulton M. RPE lipofuscin and its role in retinal pathobiology. *Exp Eye Res.* 2005;80:595-606.

43. Huang RF, Huang SM, Lin BS, Hung CY, Lu HT. N-acetylcysteine, vitamin C and vitamin E diminish homocysteine thiolactone-induced apoptosis in human promyeloid HL-60 cells. *J Nutr.* 2002; 132:2151-2156.

44. Guaiquil VH, Vera JC, Golde DW. Mechanism of Vitamin C inhibition of cell death induced by oxidative stress in glutathione-depleted HL-60 cells. *J Biol Chem.* 2001;276:40955-40961.

45. Liang F-Q, Alssadi R, Morehead P, Awasthi YC, Godley BF. Enhanced expression of glutathione-S-transferase A1-1 protects against oxidative stress in human retinal pigment epithelial cells. *Exp Eye Res.* 2005;80:113-119.